

Quantum quench dynamics in Dicke superradiance models

Michal Kloc,* Pavel Stránský, and Pavel Cejnar

*Institute of Particle and Nuclear Physics, Faculty of Mathematics and Physics,
Charles University, V Holešovičkách 2, Prague, 18000, Czech Republic*

(Dated: December 14, 2024)

We study the quantum quench dynamics in an extended version of the Dicke model where an additional parameter allows a smooth transition to the integrable Tavis-Cummings regime. We focus on the influence of various quantum phases and excited-state quantum phase transitions (ESQPTs) on the survival probability of the initial state. We show that, depending on the quench protocol, an ESQPT can either stabilize the initial state or, on the contrary, speed up its decay to the equilibrated regime. Quantum chaos smears out the manifestations of ESQPTs in quench dynamics, therefore significant effects can only be observed in integrable or weakly chaotic settings. Similar features are present also in the post-quench dynamics of some observables.

I. INTRODUCTION

The advent of quantum simulators opened routes to laboratory realizations of artificial quantum systems designed either to implement certain utilizable functions, or to demonstrate some fundamental principles [1, 2]. Examples include efforts to build an efficient quantum computer (see, e.g., Ref. [3]) or experiments with quantum phase transitions (see, e.g., Refs. [4–6]). An important mode of use of quantum simulators lies in probing the dynamics of quantum systems far from thermodynamical equilibrium [7, 8]. This is often achieved via a protocol called quantum quench, which in its sudden form consists in the following steps: (a) take a system described by Hamiltonian \hat{H}_i and prepare it in an eigenstate $|\psi_i\rangle$, (b) suddenly switch the Hamiltonian to \hat{H}_f , and (c) with increasing time t , measure the probability $P(t)$ of finding the initial state $|\psi_i\rangle$ in the state evolved from it by \hat{H}_f . It is usually assumed that the initial and final Hamiltonians are members of the same family depending on an external parameter λ , so $\hat{H}_i \equiv \hat{H}(\lambda_i)$ and $\hat{H}_f \equiv \hat{H}(\lambda_f)$ with λ_i and λ_f denoting initial and final parameter values.

The evolution of the initial-state survival probability $P(t)$, a so-called Loschmidt echo [9, 10], is entirely encoded in the energy distribution of the initial state expressed in the final Hamiltonian eigenstates. At first, $P(t)$ drops with a rate related just to the final energy dispersion. However, at later stages of the evolution, rather complex dynamical regimes occur which gradually disclose more and more subtle details of the final energy distribution. Correlations between individual final energy levels as well as those between the corresponding occupation probabilities become apparent at these stages. Although the medium- and long-time evolution is usually characterized by a very low average of the survival probability, sharp peaks of $P(t)$ are repeatedly observed, indicating sudden revivals of the initial state.

The quench dynamics in complex quantum systems currently represents a subject of intense theoretical and

experimental research, see, e.g., Refs. [6, 11–21]. An important direction of this research is aimed at dynamical imprints of various forms of quantum criticality that emerge in the infinite-size limit of some systems. For example, the so-called Dynamical Quantum Phase Transition (DQPT) shows up as a non-analyticity observed directly in the Loschmidt echo as a function of time [6, 17]. Also relevant for the quench dynamics are the concepts of ground-state Quantum Phase Transition (QPT) [22, 23] and Excited-State Quantum Phase Transition (ESQPT) [24–28]. Since these are rooted in non-analytic properties of the system's stationary states (ground or excited states) taken as a function of the control parameter, their effect in quench dynamics is not seen as a sharp-time anomaly like in the DQPT case, but rather shows as a qualitative change of the quench dynamics with varying difference $\Delta\lambda = \lambda_f - \lambda_i$. The changes appear if the parameter shift connects different quantum phases of the system. In spite of numerous theoretical efforts to clarify the relations between (ES)QPTs and quench dynamics (see, e.g., Refs. [11, 12, 14, 15, 18] for QPTs and [13, 16, 19] for ESQPTs), the problem still remains open for further investigation.

In this paper, we address this problem, particularly that of the ESQPT influence, by analyzing the quench dynamics in a model generalizing the Dicke superradiance phenomenon in cavity QED systems [29–31]. The model contains a QPT [32] and several types of ESQPTs [13, 33–38]. Its ground-state critical behavior was demonstrated experimentally [5]. We show that the effect of ESQPTs on the quench dynamics strongly depends on the ESQPT type (in the sense of the classification described in Ref. [28]) and on the quench protocol (selection of the initial state and size of the parameter change). The effect is most pronounced in the integrable Tavis-Cummings regime [39], in which the dynamics becomes effectively determined by a single degree of freedom, but can be observed also in the full (non-integrable) regime.

The plan of the paper is as follows: In Section II, we introduce an extended version of Dicke model (Sec. II A), that will be employed in this work, and outline the general theoretical background on the quench dynamics (Sec. II B). In Section III, we describe numerical re-

* E-mail address: kloc@ipnp.troja.mff.cuni.cz

sults on the quench dynamic gained within the model in its integrable (Sec. III A) and non-integrable regimes (Sec. III B). We focus on two types of quench protocols named forward and backward protocols. Section IV brings a summary.

II. THEORETICAL BACKGROUND

A. The extended Dicke model

The Dicke model [29] was formulated to describe an idealized interaction of an ensemble of N two-level atoms with one-mode electromagnetic field. The original intention was to demonstrate the dynamical superradiance phenomenon, i.e., coherent radiation induced by collective behavior of atoms in the regime of weak atom-field coupling. Later it turned out that in the strong coupling regime, the model exhibits another form of superradiance, namely a thermal phase transition [30, 31] and, in the zero-temperature limit, the corresponding QPT [32] to an equilibrium superradiant phase. A route to laboratory realizations of the cavity QED system with strong atom-field coupling was proposed in Ref. [40] and led to successful experiments with the superradiant QPT reported in Ref. [5].

We use here the so-called Extended Dicke Model [33, 34, 37, 41] with the Hamiltonian

$$\hat{H} = \omega \hat{b}^\dagger \hat{b} + \omega_0 \hat{J}_z + \frac{\lambda}{\sqrt{N}} \left[\hat{b}^\dagger \hat{J}_- + \hat{b} \hat{J}_+ + \delta \left(\hat{b}^\dagger \hat{J}_+ + \hat{b} \hat{J}_- \right) \right]. \quad (1)$$

Here, \hat{b}^\dagger and \hat{b} stand for creation and annihilation operators of the bosonic field (photons) while \hat{J}_\pm and \hat{J}_z represent collective quasi-spin operators affecting the ensemble of atoms. These are written as $\hat{J}_\bullet = \sum_{k=1}^N \hat{\sigma}_\bullet^k / 2$ (with the symbol \bullet standing for $z, +, -$), where $\hat{\sigma}_\bullet^k$ is the Pauli matrix acting on the k th atom whose lower and upper states read as $\begin{pmatrix} 1 \\ 0 \end{pmatrix}$ and $\begin{pmatrix} 0 \\ 1 \end{pmatrix}$, respectively [so, for example, $\hat{\sigma}_+^k / 2 = (\hat{\sigma}_x^k + i\hat{\sigma}_y^k) / 2$ excites the k th atom from the lower to the upper state etc.]. The first two terms in Eq. (1) represent the free field (with a single boson energy ω) and free atoms (with a single atom excitation energy ω_0), while the third term describes an atom-field interaction with an overall strength $\lambda \in [0, \infty)$ and an additional parameter $\delta \in [0, 1]$ which scales the so-called counter-rotating terms. The variation of δ induces a smooth crossover from the Tavis-Cummings regime [39] with $\delta = 0$ (full neglect of the counter-rotating terms) to the original Dicke regime [29] with $\delta = 1$.

Note that the use of collective quasi-spin operators in the interaction term is based on the assumption that the size of the atomic ensemble is much smaller the wavelength of radiation, so that the interaction is uniform for all atoms. Since \hat{J}^2 commutes with the Hamiltonian (1), the dynamics does not mix subspaces with different quantum numbers j of \hat{J}^2 . We therefore select a single- j subspace, namely that with the maximal value

$j = N/2$, which is fully symmetric with respect to the exchange of atoms (subspaces with lower values of j appear in numerous replicas differing by the type of exchange symmetry) [42]. So all physical states $|\psi\rangle$ can be expressed as linear combinations of the basis states $|n\rangle|m\rangle$, where $n = 0, 1, 2, \dots$ is the number of bosons and $m = -j, -j+1, \dots, +j$ the quasi-spin z -projection.

The classical limit of Hamiltonian (1) can be realized in terms of two pairs of canonically conjugate coordinate and momentum variables, hence the model has in general two degrees of freedom: $f = 2$ [32, 34]. One of them is associated with the field states; the corresponding part of the phase space is a plane. The other represents the collective atomic states; their phase space is the Bloch sphere. Details can be found, e.g., in Refs. [37, 38]. The minimum of the classical energy landscape in the whole phase space, i.e., the lowest stationary point of the system, corresponds to the energy of the quantum ground state in the $N \rightarrow \infty$ limit. It can be written as

$$\frac{E_{\text{g.s.}}}{\omega_0 j} = \begin{cases} -1 & \text{for } \lambda \in [0, \lambda_c), \\ -\frac{1}{2} \left(\frac{\lambda_c^2}{\lambda^2} + \frac{\lambda^2}{\lambda_c^2} \right) & \text{for } \lambda \in [\lambda_c, \infty), \end{cases} \quad (2)$$

where the critical parameter value

$$\lambda_c = \frac{\sqrt{\omega\omega_0}}{1+\delta} \quad (3)$$

sets a second-order ground-state QPT, where $d^2 E_{\text{g.s.}} / d\lambda^2$ changes discontinuously.

Higher (unstable or quasi-stable) stationary points of the classical Hamiltonian demarcate the ESQPTs of the model. Detailed analyses can be found in Refs. [34, 37]. One of the ESQPT critical borderlines in the plane parameter $\lambda \times \text{energy } E$ can be written as

$$\frac{E_{c1}}{\omega_0 j} = \begin{cases} -1 & \text{for } \lambda \in [\lambda_c, \lambda_0), \\ -\frac{1}{2} \left(\frac{\lambda_0^2}{\lambda^2} + \frac{\lambda^2}{\lambda_0^2} \right) & \text{for } \lambda \in [\lambda_0, \infty), \end{cases} \quad (4)$$

$$\lambda_0 = \frac{\sqrt{\omega\omega_0}}{1-\delta}.$$

The energy (4) is associated with a saddle point of the energy landscape. Therefore, according to the classification described in Ref. [28], it corresponds to an ESQPT of type $(f, r) = (2, 1)$, where r is the rank of the non-degenerate stationary point (number of negative eigenvalues of the Hessian matrix). This leads to a logarithmic divergence of the first derivative $d\rho/dE$ of the smoothed level density $\rho(E)$ at $E = E_{c1}$ (that is a step-like but continuous behavior of ρ at this energy) [27, 28].

Two other ESQPTs appear at energies [34, 37]

$$\frac{E_{c2}}{\omega_0 j} = -1 \quad \text{for } \lambda \in [\lambda_0, \infty), \quad (5)$$

$$\frac{E_{c3}}{\omega_0 j} = +1 \quad \text{for } \lambda \in [0, \infty). \quad (6)$$

They are both of the type $(f, r) = (2, 2)$ and show as jumps of the first derivative $d\rho/dE$ of the smoothed level density (i.e., breaks of ρ) at E_{c1} and E_{c2} [27, 28].

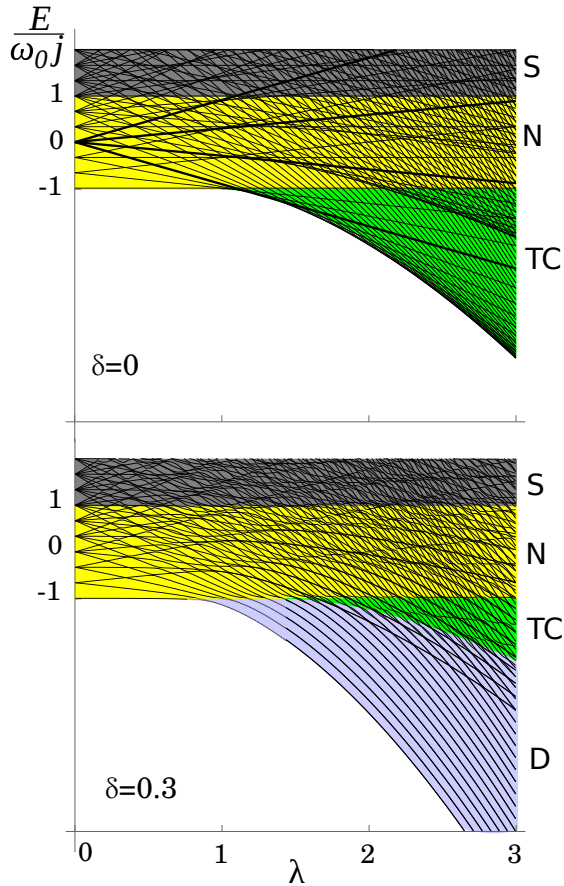


FIG. 1. (Color online) Level dynamics and quantum phase diagrams of the extended Dicke Hamiltonian (1) with $\delta = 0$ (upper panel) and $\delta = 0.3$ (lower panel), both for $\omega = \omega_0 = 1$. The ground-state QPTs are at $\lambda_c = 1$ for $\delta = 0$ and at $\lambda_c \approx 0.77$ for $\delta = 0.3$. Quantum phases D (Dicke), TC (Tavis-Cummings), N (Normal) and S (Saturated) are marked by colors, ESQPT borderlines coincide with the phase boundaries. Quantum spectra are drawn for $j = 3$. In the $\delta = 0$ panel, the $M = 3$ states are plotted by thicker lines to show that levels from different M -subspaces mutually cross.

The diagrams showing individual energy levels in the $\lambda \times E$ plane for a finite- N realization of the $\delta = 0$ and $\delta \neq 0$ models together with the $N \rightarrow \infty$ ESQPT borderlines (4), (5) and (6) are given in Fig. 1. The domains in between the ESQPT borderlines define quantum phases of the system. In Fig. 1 they are marked by different colors and abbreviated as D (Dicke), TC (Tavis-Cummings), N (Normal) and S (Saturated). The reasoning for this notation and a more detailed discussion can be found in Ref. [37]. Note that quantum phases cannot, in general, be distinguished by some order parameters (expectation values of suitably selected observables in individual eigenstates), but rather by different energy dependences (trends) of these expectation values smoothed over neighboring eigenstates [37, 42].

In the Tavis-Cummings $\delta = 0$ limit of the model [39], the treatment of phases can be qualitatively simplified.

In this case, the Hamiltonian (1) has an additional integral of motion

$$\hat{M} = \hat{b}^\dagger \hat{b} + \hat{J}_z + j \quad (7)$$

and the system is integrable [note that a general $\delta \neq 0$ Hamiltonian conserves only the parity $\hat{\Pi} = \exp(i\pi\hat{M})$]. The value of the conserved quantity can be written as $M = n + n^*$, where n is the number of bosons and $n^* = m + j$ the number of excited atoms. The total spectrum of quantum energy levels for the $\delta = 0$ system with any λ is comprised of mutually non-interacting sub-spectra with different values of $M = 0, 1, 2, \dots$ (see the upper panel of Fig. 1). Each of these spectra separately can be subject (in the $N \rightarrow \infty$ limit) to a semi-classical phase transitional analysis. To do so, it is convenient to use a canonical transformation that reduces the number of effective degrees of freedom of the $\delta = 0$ system to $f = 1$ [37, 38]. The transformed classical Hamiltonian depends only on one pair of new conjugate variables and on the conserved quantity M , thus allows one to identify stationary and quasi-stationary points for different values of M .

The results of the semi-classical analysis of the $\delta = 0$ model are the following [37, 38]: While the subspaces with $M \neq N$ show no critical effects, the one with $M = N$ has both a QPT and an ESQPT. Indeed, the energy of the lowest state in the $M = N$ subspace in the $N \rightarrow \infty$ limit for the $\omega > \omega_0$ hierarchy is given by

$$\frac{E_{l.s.}}{\omega_0 j} = \begin{cases} +1 & \lambda \leq \bar{\lambda}_c, \\ +1 - \frac{4}{\omega_0} g(\lambda) \left[\lambda \sqrt{1 - g(\lambda)} - \bar{\lambda}_c \right] & \lambda > \bar{\lambda}_c, \end{cases} \quad (8)$$

$$g(\lambda) = \frac{2}{3} - \frac{2}{9} \left(\frac{\bar{\lambda}_c}{\lambda} \right)^2 - \frac{2}{9} \frac{\bar{\lambda}_c}{\lambda} \sqrt{\left(\frac{\bar{\lambda}_c}{\lambda} \right)^2 + 3},$$

where the critical coupling

$$\bar{\lambda}_c = \frac{\omega - \omega_0}{2} \quad (9)$$

marks a discontinuity of $d^2 E_{l.s.}/d\lambda^2$, which can be interpreted as the second-order QPT in the $M = N$ subspace [13]. An associated ESQPT appears at the critical energy

$$\frac{E_{c4}}{\omega_0 j} = +1 \quad \text{for } \lambda \in [\bar{\lambda}_c, \infty), \quad (10)$$

where one observes divergence of the smoothed level density ρ in the $M = N$ subspace. Since the classical Hamiltonian is not analytic in this stationary point, the ESQPT classification according to Ref. [28] does not work here. Nevertheless, the observed signatures of the present ESQPT are quite similar to the case $(f, r) = (1, 1)$, which is most studied in literature, see, e.g., Refs. [16, 19, 24, 25, 43–46].

The level dynamics for two M -subspaces (including the critical one) of the $\delta = 0$ model are shown in Fig. 2. In the $M = N$ subspace we indicate two quantum phases separated by the ESQPT above $\bar{\lambda}_c$. The phase abbreviated by A (Atomic) is characterized by a growing average $\langle n^* \rangle$

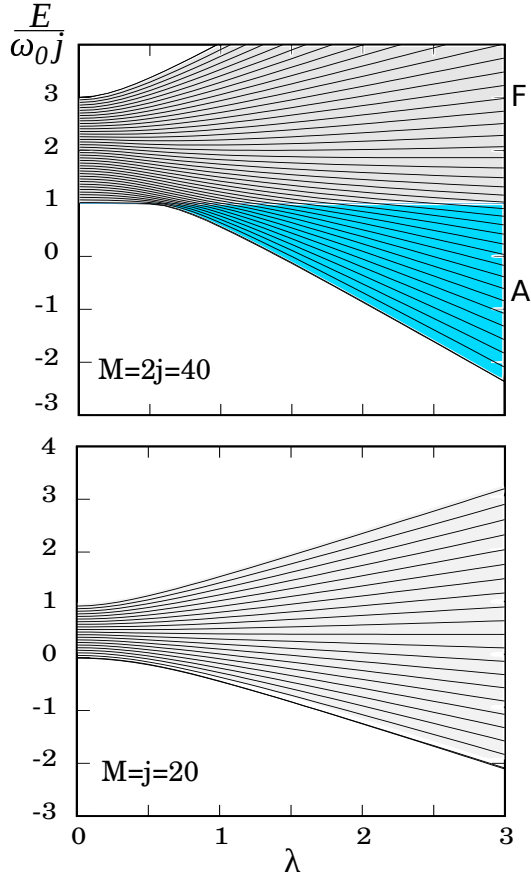


FIG. 2. (Color online) Energy spectra of two M -subspaces of the $\delta = 0$ model with $N = 2j = 40$ and $\omega_0 = \omega/2 = 1$. The upper panel shows a critical subspace $M = 2j$ with a QPT and ESQPT. Quantum phases are distinguished by colors and acronyms A (Atomic) and F (Field). The lower panel shows a non-critical subspace $M = j$.

of the number of atomic excitations in individual eigenstates with increasing energy. The average $\langle n^* \rangle$ reaches its maximum right at the ESQPT critical energy and then decreases [13], which allows us to denote the quantum phase above the ESQPT by the acronym F (Field). In this phase, the increase of energy is correlated with a growing average $\langle n \rangle$ of the number of bosons.

B. Quantum quench dynamics

Consider a quantum system with discrete energy spectrum described by a general Hamiltonian

$$\hat{H}(\lambda) = \hat{H}_0 + \lambda \hat{V} \quad (11)$$

depending linearly on a control parameter λ . As in the case of the extended Dicke model (1), the term H_0 represents a free Hamiltonian while V is an interaction. We assume $[\hat{H}_0, \hat{V}] \neq 0$ since otherwise everything would be trivial. Suppose that the system is initially prepared in the k th eigenstate $|\phi_k(\lambda_i)\rangle \equiv |\phi_{ik}\rangle \equiv |\psi_i\rangle$ with energy

$E_k(\lambda_i) \equiv E_{ik} \equiv E_i$ associated with the initial Hamiltonian $\hat{H}(\lambda_i) \equiv \hat{H}_i$, and that the control parameter is suddenly changed from λ_i to λ_f . The initial state is no more an eigenstate of the final Hamiltonian $\hat{H}(\lambda_f) \equiv \hat{H}_f$ and thus undergoes a non-trivial evolution with time t :

$$|\psi_f(t)\rangle = e^{-i\hat{H}_f t} |\psi_i\rangle, \quad (12)$$

where we assume $\hbar = 1$. The decay and recurrences of the initial state can be monitored by the survival amplitude $A(t) = \langle \psi_i | \psi_f(t) \rangle$ (here and below we assume that all states are normalized). The survival probability $P(t) = |A(t)|^2$ is sometimes called Loschmidt echo (as it can be interpreted as the probability of the initial state recovery after the forward evolution by \hat{H}_f and a backward evolution by \hat{H}_i) and is related to a more general quantity called fidelity [9, 10].

Let us introduce the basis of the final Hamiltonian eigenvectors $|\phi_l(\lambda_f)\rangle \equiv |\phi_{fl}\rangle$ and the corresponding set of eigenvalues E_{fl} . The distribution of the initial state in the final Hamiltonian eigenstates is expressed by the strength function (also called the local density of states)

$$S(E) = \sum_l \frac{|\langle \psi_i | \phi_{fl} \rangle|^2}{|s_l|^2} \delta(E - E_{fl}). \quad (13)$$

It represents a probability distribution for energy after the shift $\lambda_i \rightarrow \lambda_f$, or shortly a distribution of final energy in the initial state. Besides the smoothened shape of the strength function, important information is contained also in its autocorrelation function:

$$\begin{aligned} C(E) &= \sum_l \sum_{l'} |s_l|^2 |s_{l'}|^2 \delta(E_{fl} - E_{fl} - E) \\ &= \int dE' S(E') S(E' + E). \end{aligned} \quad (14)$$

A trivial calculation reveals that the Loschmidt echo

$$\begin{aligned} P(t) &= \left| \sum_l |s_l|^2 e^{-iE_{fl} t} \right|^2 \\ &= \underbrace{\sum_l |s_l|^4}_{\mathcal{N}^{-1}} + 2 \sum_l \sum_{l'(<l)} |s_l|^2 |s_{l'}|^2 \cos[(E_l - E_{l'})t] \end{aligned} \quad (15)$$

can be expressed via the Fourier transforms of both the strength function and its autocorrelation function:

$$P(t) = \left| \int dE S(E) e^{-iEt} \right|^2 = \int dE C(E) e^{+iEt}. \quad (16)$$

This turns out important for the interpretation of the quantum quench dynamics in various situations. Note that the quantity $\mathcal{N} = 1/\sum_l |s_l|^4$, called the participation ratio, expresses a principal number of components of the strength function (13). It varies from $\mathcal{N} = 1$, for a perfectly localized strength function with only a single non-zero coefficient s_l , to $\mathcal{N} \rightarrow \infty$, for totally de-localized

strength functions with components uniformly spread over an asymptotically increasing number of states.

The average and variance of the distribution (13) can be determined from the relation $\hat{H}_f = \hat{H}_i + (\Delta\lambda) \hat{V}$ (where $\Delta\lambda = \lambda_f - \lambda_i$), which follows from the linearity of Hamiltonian (11). The average is given by

$$\begin{aligned} \langle E_f \rangle_i &= \int dE S(E) E = \langle \psi_i | \hat{H}_f | \psi_i \rangle \\ &= E_i + (\Delta\lambda) \langle V \rangle_i, \end{aligned} \quad (17)$$

where $\langle V \rangle_i = \langle \psi_i | \hat{V} | \psi_i \rangle$, while the variance reads

$$\begin{aligned} \langle\langle E_f^2 \rangle\rangle_i &= \int dE S(E) (E - \langle E_f \rangle_i)^2 \\ &= \langle \psi_i | \hat{H}_f^2 | \psi_i \rangle - \langle \psi_i | \hat{H}_f | \psi_i \rangle^2 = (\Delta\lambda)^2 \langle\langle V^2 \rangle\rangle_i, \end{aligned} \quad (18)$$

where $\langle\langle V^2 \rangle\rangle_i = \langle \psi_i | \hat{V}^2 | \psi_i \rangle - \langle \psi_i | \hat{V} | \psi_i \rangle^2$. Due to the Hellmann-Feynman formula $\langle V \rangle_i = dE_i/d\lambda$, the relation (17) can be used to determine the final energy average, i.e., a centroid of the distribution (13), from the position and tangent of the selected energy level at the initial parameter value. This allows one to design specific quench protocols that probe selected parts of the spectrum of the final Hamiltonian, for example, different quantum phases of the system and various ESQPT critical domains [13]. However, according to Eq. (18), the final energy variance, i.e., squared width of the distribution (13), is proportional to the variance of V in the initial state and grows with the square of $\Delta\lambda$. This sets unavoidable limits to the probing procedure since the dispersion of the final energy distribution implies averaging of the response over a broader interval of the spectrum, hence reduces the resolution of the procedure.

The evolution of the Loschmidt echo on various time scales defines different regimes of the quench dynamics [9, 10, 20]. They are governed by physical mechanisms that naturally follow from an increasing energy resolution with which the strength function (13) is being reflected by the evolving system at the given instant of time. The regimes of quantum quench dynamics can be schematically described as follows:

(a) Ultra-short time regime, $t \ll t_s$, where

$$t_s = \frac{1}{\sqrt{\langle\langle E_f^2 \rangle\rangle_i}} \quad (19)$$

is the time derived from the final energy dispersion (18): At this time scale, the system can feel merely the width of the strength function and decays according to the simple quadratic formula $P(t) \approx 1 - (t/t_s)^2 + \dots$. This stage of evolution carries no information on the final Hamiltonian.

(b) Short- and medium-time regime, from $t \sim t_s$ up to times $t \ll t_H$ well below the Heisenberg scale set by

$$t_H = \frac{2\pi}{\sum_l \frac{1}{2} [|s_{l+1}|^2 + |s_l|^2] [E_{f(l+1)} - E_{fl}]} = \frac{2\pi}{\langle\Delta E_f\rangle_i} \quad (20)$$

where $\langle\Delta E_f\rangle_i$ is an average spacing of the final energy levels in the initial state distribution: In this regime,

the energy resolution becomes sufficient to distinguish an outline shape of the strength function (13) as well as some of its correlation properties given by Eq. (14). Qualified estimates of the shape in various situations predict an initially exponential, Gaussian or sub-Gaussian decrease of the survival probability [20]. The first dip of $P(t)$ (a “survival collapse”) is sometimes followed by modulated oscillations with a power-law decrease of their amplitude (related for instance to low- and/or high-energy edges of the strength function).

(c) Long-time regime, around $t \sim t_H$: At this time scale, the system gradually resolves the discrete structure of the strength function, from smaller to larger level density domains. Power-law modulated oscillations can appear also at this stage, being connected with the behavior of the autocorrelation function for small energy differences. They may be followed by a so-called correlation hole (a long-lasting suppression of the survival probability below its asymptotic-time average), which reflects strong correlations of individual levels in chaotic systems.

(d) Ultra-long time regime, $t \gg t_H$: The infinite-time average and variance of the function $P(t)$ in Eq. (15) read

$$\overline{P(t)} = \mathcal{N}^{-1}, \quad (21)$$

$$\overline{P(t)^2} - \overline{P(t)}^2 = \mathcal{N}^{-2} - \sum_l |s_l|^8, \quad (22)$$

where bars represent time averaging of the respective quantities according to $\overline{g(t)} = \lim_{T \rightarrow \infty} \int_0^T g(t) dt / T$. So in the very long time perspective, the Loschmidt echo can be seen as fluctuations around the “saturation value” (21) with standard deviation given by the the square root of (22). Both these quantities decrease with the degree of fragmentation of the corresponding strength function (13). The sum in Eq. (22) is even a sharper measure of fragmentation than the inverse participation ratio \mathcal{N}^{-1} discussed before. Indeed, for maximally delocalized strength function it gives contribution of the size $\sim \mathcal{N}^{-3}$.

Despite a usually low average (21), the ultra-long time regime unavoidably includes also sharp peaks of $P(t)$ reaching values even very close to unity. These partial revivals of the initial state demonstrate the well-known quantum recurrence theorem [47], which guarantees that for any initial state of a system with discrete spectrum and for an arbitrary degree of precision there exists a time at which the evolved state restores the initial one with this precision. As follows from Eq. (22), a higher frequency of recurrences is expected for less fragmented strength functions and vice versa.

A valuable insight into the Loschmidt echo evolution can be gained from the quasi-classical picture of quantum dynamics. Associating with the state $|\psi_f(t)\rangle$ at any stage of its evolution the Wigner phase-space distribution function $W(q, p, t)$, we can rewrite the survival probability as

$$P(t) = 2\pi \iint dq dp W(q, p, t) W(q, p, 0), \quad (23)$$

where q and p stand for f -dimensional vectors of mutually conjugate coordinates and momenta, respectively. Assume that $W(q, p, t)$ is classical-like (i.e., shows only negligible domains with negative values) or is transformed to such form by a convenient smoothing procedure $W(q, p, t) \rightarrow \bar{W}(q, p, t)$. Then the evolution can be approximated by means of the equations of motions derived from the classical Hamiltonian function $H_f(q, p)$ corresponding to \hat{H}_f .

The classical treatment of the smooth(ed) Wigner function $\bar{W}(q, p, t)$ and its evolution allows one to estimate possible signatures of classical stationary points in the Loschmidt echo $P(t)$, and therefore to partly anticipate an influence of QPTs and ESQPTs on the quench dynamics. Consider a stationary point (q_s, p_s) of the function H_f at energy $E_s = H_f(q_s, p_s)$. If E_s belongs to the support of a smoothed strength function $\bar{S}(E)$, some effects of the stationary point may be seen in $P(t)$ for $t \lesssim t_H$. The form of these effects is expected to depend on whether the stationary point (q_s, p_s) is located within the phase-space domain where the initial distribution $\bar{W}(q, p, 0)$ yields considerable contributions, or whether the stationary point is outside that domain. If the first case, the decay of the survival probability (23) gets slowed down at its initial stage, $t \lesssim t_s$, due to the slow classical dynamics around (q_s, p_s) . A clear demonstration of this behavior within the extended Dicke model will be presented in Secs. III A 1 and III B 1.

On the other hand, if the stationary point is located outside the domain with large values of $\bar{W}(q, p, 0)$, the short-time decay of $P(t)$ remains unaffected. Nevertheless, an indirect effect may be observed at some later stages of the $P(t)$ evolution, when the stationary point (q_s, p_s) prevents the return of a certain fraction of the $\bar{W}(q, p, t)$ distribution (that with energy close to E_s) back to the initial phase-space domain. Then we may expect a partial reduction of the Loschmidt echo $P(t)$ for times comparable with the Heisenberg scale, $t \sim t_H$, which coincides with an average classical return time. Indications of such behavior will be indeed discussed in Secs. III A 2 and III B 2, but we stress here that the reduction size (the possibility to actually observe any effect) strongly depends on the degree of stability (chaos) of classical motions generated by $H_f(q, p)$ in the relevant phase-space domain.

III. NUMERICAL RESULTS

In this section, numerical results on the quantum quench dynamics in the extended Dicke model with Hamiltonian (1) will be analyzed. Subsection III A deals with the quenches in M -subspaces of the integrable $\delta = 0$ (Tavis-Cummings) regime where the dynamics is effectively reduced to one degree of freedom. Subsection III B is focused on the quenches in the full $\delta \neq 0$ model with two degrees of freedom.

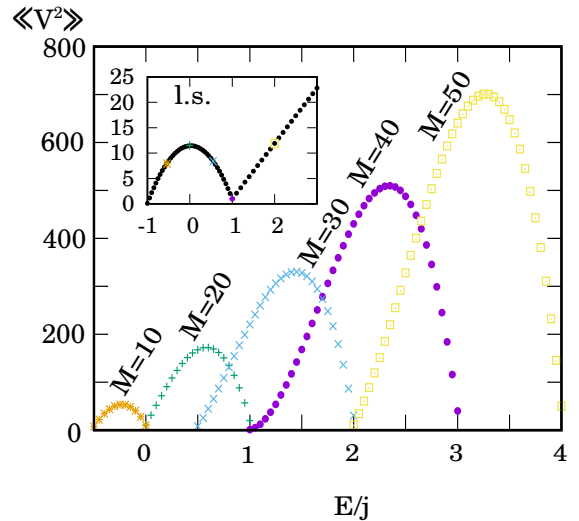


FIG. 3. (Color online) Dispersion $\langle\langle V^2 \rangle\rangle_i$ from Eq. (24) in the unperturbed eigenstates $|\psi_i\rangle = |n\rangle|m\rangle$ of the $\delta = 0$ model plotted against their energies. Parameters of the system are $\omega = 2, \omega_0 = 1, j = 20$. The inset shows $\langle\langle V^2 \rangle\rangle_i$ in the lowest states from all M -subspaces. The states involved in the main panel are marked in the inset by the respective symbols.

A. Integrable $\delta = 0$ regime

1. Forward quench protocols, $f = 1$

The evolution of the Loschmidt echo strongly depends on the quench protocol, that is on the selection of the initial state and on the size of the parameter change. In the forward quench protocols (FQPs) we set initial states as various eigenstates of the unperturbed $\lambda_i = 0$ Hamiltonian and choose the final value $\lambda_f > 0$.

The decay rate at ultra-short and short times of such initial states can be estimated using Eqs. (18) and (19). In the detuned system $\omega \neq \omega_0$ (the initial eigenstates are non-degenerate, hence $|\psi_i\rangle = |n\rangle|m\rangle$), a simple formula for the dispersion of the interaction Hamiltonian term can be obtained:

$$\langle\langle V^2 \rangle\rangle_i = \frac{(1 + \delta^2)(j^2 - m^2 + j)(2n + 1) + (1 - \delta^2)m}{2j}. \quad (24)$$

In Fig. 3 we show $\langle\langle V^2 \rangle\rangle_i$ in multiple eigenstates belonging to several M -subspaces for $j = 20$. For all the subspaces we observe a similar dependence—the states closer to the edges of the spectrum have smaller dispersion than the ones in the middle and therefore their decay is slower. However, a closer look reveals an anomaly for the critical subspace $M = 2j = 40$. The inset of Fig. 3 depicts the dispersion of the lowest state from all subspaces with $M = 0, 1, 2, \dots$, plotted against their energies $E_{l.s.}(M) = \omega(M - j) - (\omega - \omega_0)j$. The leftmost point corresponding to the global ground state has $\langle\langle V^2 \rangle\rangle_i = 0$. Indeed, as it is the only member of the $M = 0$ subspace it cannot decay. However, small values of dispersion are reached

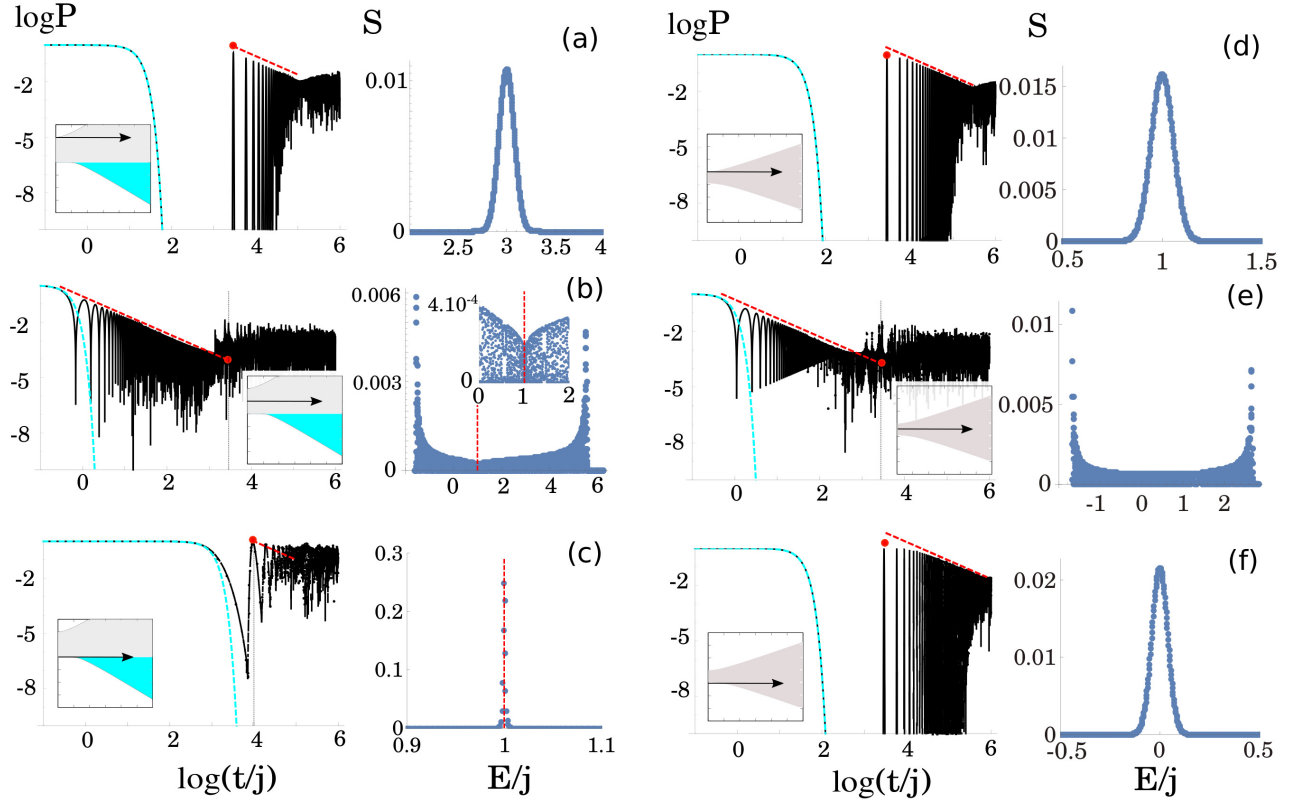


FIG. 4. (Color online) The Loschmidt echo and the strength function corresponding to the FQPs of the $\delta = 0$ model with $j = 2000$ in off-resonant setting $\omega = 2, \omega_0 = 1$. The critical $M = 2j$ subspace is shown in panels (a)–(c), a non-critical $M = j$ subspace in panels (d)–(f). In all the cases, $\lambda_i = 0$ and $\lambda_f = 2.5$, the quench protocol is visualized by an arrow in the respective phase diagram. The real decay (black curves) is compared with the Gaussian decay (the light-blue dashed curves), the Heisenberg time t_H is marked with the red bullets, and the $1/t$ decay of oscillations is marked with the red dashed lines. In the strength function plots, the position of the ESQPT is indicated by vertical lines.

also for the M -subspaces close to the critical one with $\langle V^2 \rangle_i = 1/2j$, which indicates an asymptotically slow decay of the respective initial states in the $j \rightarrow \infty$ limit.

Let us now proceed to concrete examples of FQPs within two M -subspaces, the critical one with $M = 2j$ and the non-critical with $M = j$. In the following we consider $j = 2000$. Fig. 4 depicts both the Loschmidt echo and the strength function for several initial states from the above mentioned subspaces.

In the first row of Fig. 4 (panels a and d) we compare the highest excited states. The envelope of the strength function has a Gaussian shape giving rise to an initial Gaussian decay of the Loschmidt echo [20]. After the initial decay, strong revivals appear at about the Heisenberg time t_H . Their amplitude decreases as $\propto 1/t$ until the saturation regime around $P(t) \sim \mathcal{N}^{-1}$ is reached. The power-law modulation $\propto 1/t^\alpha$ of the oscillations with various exponents α was observed in various systems and has been attributed to several specific mechanisms [20, 48]. The present case $\alpha = 1$ results from two conditions: an approximately Gaussian envelope of the strength function and its discrete energy sampling

$$E_{tl} \approx e_0 + e_1 l + e_2 l^2 \quad (25)$$

with parameters e_0, e_1, e_2 satisfying $|e_2| \ll |e_1|$ [48]. As can be numerically checked, both these conditions are valid in our case.

In the second row of Fig. 4 (panels b and e) we compare the decay of $\lambda_i = 0$ initial states from the middle of $M = 2j$ and $M = j$ spectra. In both cases, the strength function has a bimodal shape with large dispersion. As a result, the initial decay is faster than Gaussian. We again observe $\propto 1/t$ modulated oscillations, but *before* the Heisenberg time t_H . In this case, the origin of the power-law dependence lies purely in the profile of the strength function, namely in its U-shaped envelope. Although the ESQPT does not visibly affect the Loschmidt echo, the inset of panel (b) shows that the strength function forms a small dip at the critical energy.

Finally, the last row of Fig. 4 (panels c and f) depicts FQPs with the lowest states from both $M = 2j$ and $M = j$ subspaces. Panel (c) shows the critical quench—the initial ground state is displaced directly into the ESQPT region (see the phase diagram inset). The initial decay is significantly slowed down (even slower than the Gaussian decay). Semiclassically this can be viewed as a slowdown of the dynamics due to the localization of the initial state

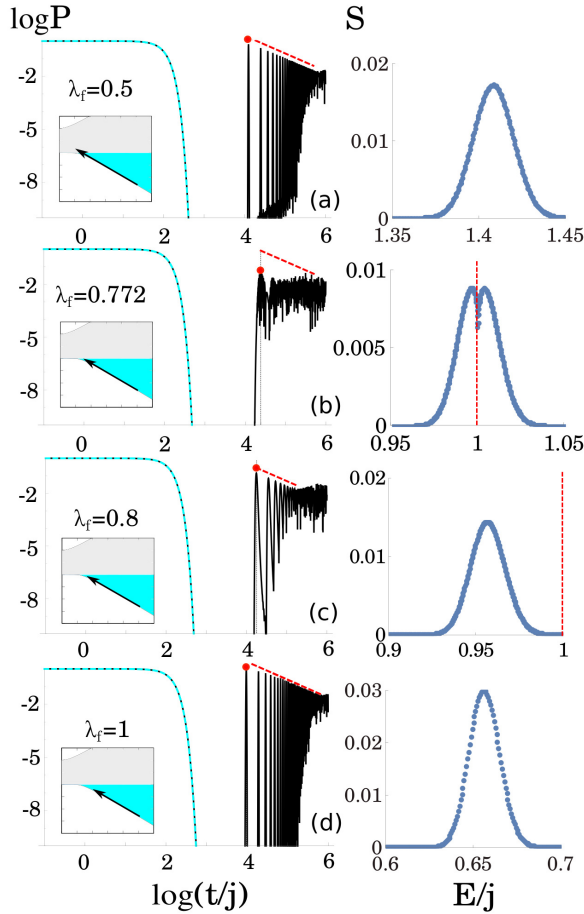


FIG. 5. (Color online) The Loschmidt echo and the strength function corresponding to the BQPs in the critical $M = 2j$ subspace of the $\delta = 0$ model. The parameters and meaning of symbols are the same as in Fig. 4.

at the stationary point (q_s, p_s) of the final Hamiltonian, see the end of Sec. II B. A very sharp strength function indicates high localization of the initial state in the final eigenbasis. As the Gaussian envelope is lost, we do not observe any power-law modulated oscillations around the Heisenberg time. On the other hand, in the non-critical subspace (panel f) we obtain a similar decay pattern as for the highest excited state (panel d) manifesting that the presence of an ESQPT is crucial for the existence of the localization. The stabilization of the initial state due to an ESQPT within a similar quench protocols in different $f = 1$ systems was also studied in Refs. [19, 21].

2. Backward quench protocols, $f = 1$

In the backward quench protocols (BQPs), we set λ_i above the critical value (in this case $\bar{\lambda}_c$) and choose various values of $\lambda_f < \lambda_i$ [13]. In Fig. 5 we consider the initial ground state at $\lambda_i = 2.5$. The Loschmidt echoes and strength functions for $\lambda_f = 0.5$ (panel a), $\lambda_f = 0.8$

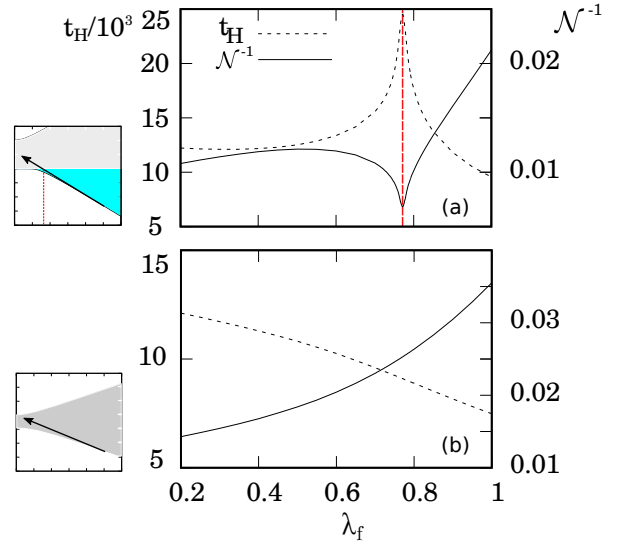


FIG. 6. (Color online) The Heisenberg time t_H and inverse participation ratio \mathcal{N}^{-1} for the BQPs in the critical $M = 2j$ (panel a) and non-critical $M = j$ (panel b) subspaces of the $\delta = 0$ model. The parameters are the same as in Fig. 4. The critical quench in panel (a) is marked with vertical line.

(c) and $\lambda_f = 1$ (d) are qualitatively similar to those in panels (a), (d) and (f) of Fig. 4. For $\lambda_f \doteq 0.772$ (panel b of Fig. 5) the strength function is centered at the ESQPT energy, so it corresponds to a critical quench. We observe a splitting of the maximum and a dip at the critical energy, cf. Fig. 4(b). The initial decay of the Loschmidt echo does not differ from the other cases in Fig. 5, but the $\propto 1/t$ dependence of revivals around the Heisenberg time t_H is not present. The reason is the violation of formula (25) because the strength function is equally distributed in two different quantum phases. On the semiclassical level, we can deduce that the stationary point (q_s, p_s) of the final Hamiltonian is located outside the support of the initial state's Wigner function, which has consequences at the $t \sim t_H$ behavior of the Loschmidt echo; see the end of Sec. II B.

As the revivals are suppressed, the evolution of the Loschmidt echo gets to the saturation regime right after the survival collapse which can be interpreted as a speed-up of the decay. This difference from the FQP case, where the ESQPT caused a longer survival, demonstrates that the quench protocol plays a crucial role for the ESQPT-induced effects.

In Fig. 6 we compare BQPs in both critical and non-critical subspaces by plotting Heisenberg time t_H and the inverse participation ratio \mathcal{N}^{-1} as a function of λ_f . We see that t_H has a sharp maximum at the critical quench which is a direct consequence of the level density increase at the ESQPT energy. The presence of the ESQPT is also captured by \mathcal{N}^{-1} as it shows a dip at the critical λ_f .

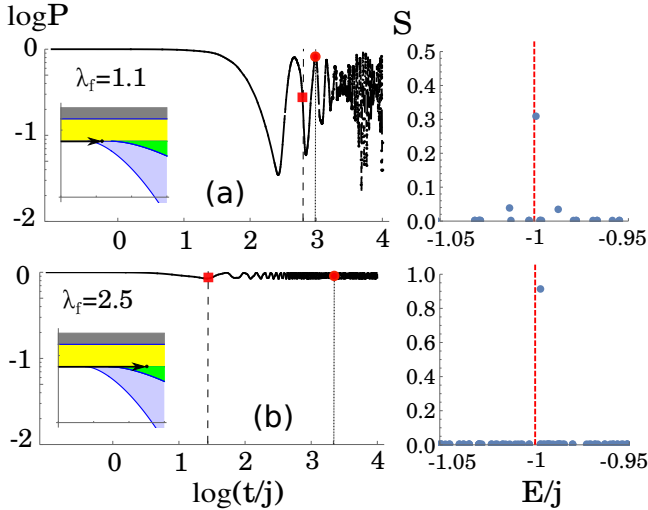


FIG. 7. (Color online) The Loschmidt echo and the strength function corresponding to the FQPs from the $\lambda_i = 0$ ground state of the $\delta = 0.3$ model with parameters $j = 20$, $\omega = \omega_0 = 1$ in the even parity sector. The standard and modified Heisenberg times t_H and t'_H are marked with the red bullet and square, respectively.

B. General $\delta \neq 0$ regime

1. Forward quench protocols, $f = 2$

We now proceed to studying the quench dynamics in a general $\delta \neq 0$ model with two degrees of freedom. We set the model parameter $\delta = 0.3$ and tune the system to resonance $\omega = \omega_0 = 1$. In contrast to the integrable case, we consider only the initial states associated with the ground state of H_i . In the FQPs, we choose the ground state at $\lambda_i = 0$ and perform a quench to $\lambda_f = 1.1$ and $\lambda_f = 2.5$, see Fig. 7. These values were selected because we want to test different types of ESQPTs (see the insets in the respective figure). Indeed, for $\lambda_f = 1.1$ the strength function is centered at the $(f, r) = (2, 1)$ ESQPT critical energy E_{c1} between the D and N phases. On the other hand, for $\lambda_f = 2.5$ the strength function is localized at the $(f, r) = (2, 2)$ ESQPT critical energy E_{c2} between the TC and N phases.

Panel (a) of Fig. 7 presents a similar decay pattern as the integrable case in Fig. 4(c). We again observe that the strength function has only a few non-zero components in the vicinity of the ESQPT energy indicating a rather high level of localization of the initial state in the final eigenbasis. However, if we increase the final parameter value to $\lambda_f = 2.5$, the localization becomes nearly perfect, see Fig. 7(b). Indeed, the $\lambda = 0$ ground state has a 96% overlap with the $\lambda = 2.5$ eigenstate closest to the ESQPT. This difference between D-N and TC-N phase borderlines has been pointed out in Ref. [37]. As a consequence, in the long-time regime the Loschmidt echo in Fig. 7(b) oscillates around a quite high value $P \approx 0.85$.

Apart from the Heisenberg time t_H from Eq. (20), we introduce a modified Heisenberg time t'_H . It is computed in the same way as t_H , but only with a reduced set of levels E_{fl} , from which we have removed those with the lowest values of $|s_l|^2$ (we have selected a threshold of 0,5% of the total strength). This definition is relevant in the situations when the initial state is only partially fragmented among the final eigenstates. In these cases, t'_H gives a better prediction on where the discrete structure of the strength function starts to play a role in quench dynamics, see Fig. 7(b), where t'_H is marked with the red square and the vertical dashed line. If the strength function is fully fragmented, t_H and t'_H tend to coincide.

2. Backward quench protocols, $f = 2$

Within the same setting of the model we employ BQPs starting with the superradiant ground state $\lambda_i = 6 > \lambda_c$. There are several ESQPTs to be tested in this way. In Fig. 8 the results for several values of λ_f are depicted. We observe an initial Gaussian decay in all cases. Further, we can see that the first revival appears roughly around time $t \sim t'_H$ (see the end of Sec. III B 1). These revivals decay in most cases as $1/t$. Apparently, this behavior of the revivals is also present in the critical quench to $\lambda_f = 3.1$ where the energy distribution is not affected by the $(f, r) = (2, 2)$ ESQPT between D and N phases (the ESQPT between S and N phase of the same type was also examined showing the same result). However, if we choose $\lambda_f = 3.27$, corresponding to critical quench to the $(f, r) = (2, 1)$ ESQPT between TC and D phases, we observe the vanishing of the $1/t$ modulated revivals. This is again due to the splitting of the strength function at the critical energy—a similar effect as in the $f = 1$ critical case, compare Fig. 8(d) with Fig. 5(b).

The strength functions in Fig. 8 have a common property that their support is only a certain subset of the final Hamiltonian spectrum (see the zero base corresponding to levels which are not populated). This can be interpreted so that the system is in a quasi-regular regime where the overlap with only some selected final states is allowed. So the modified Heisenberg time t'_H restricted on these states agrees better with the onset of revivals.

The regularity is illustrated in Fig. 9 where we present a so-called Peres lattice [49] of the final Hamiltonian. The Peres lattice depicts the spectrum of eigenstates as a mesh of points in the plane $E_l \times \langle O \rangle_l$, where E_l is energy and $\langle O \rangle_l$ an expectation value of a certain observable (here the number of photons) in the l th eigenstate. Orderly arranged points in the lattice indicate regularity of the respective eigenstates whereas disorder implies chaoticity [50]. The states populated in the critical quench from Fig. 8(d) are displayed by the highlighted dots, the size of each dot corresponds to the value $|s_l|^2$ of the strength function. We observe a localization of the populated states in the regular domain. The same is true for the other quenches in Fig. 8.

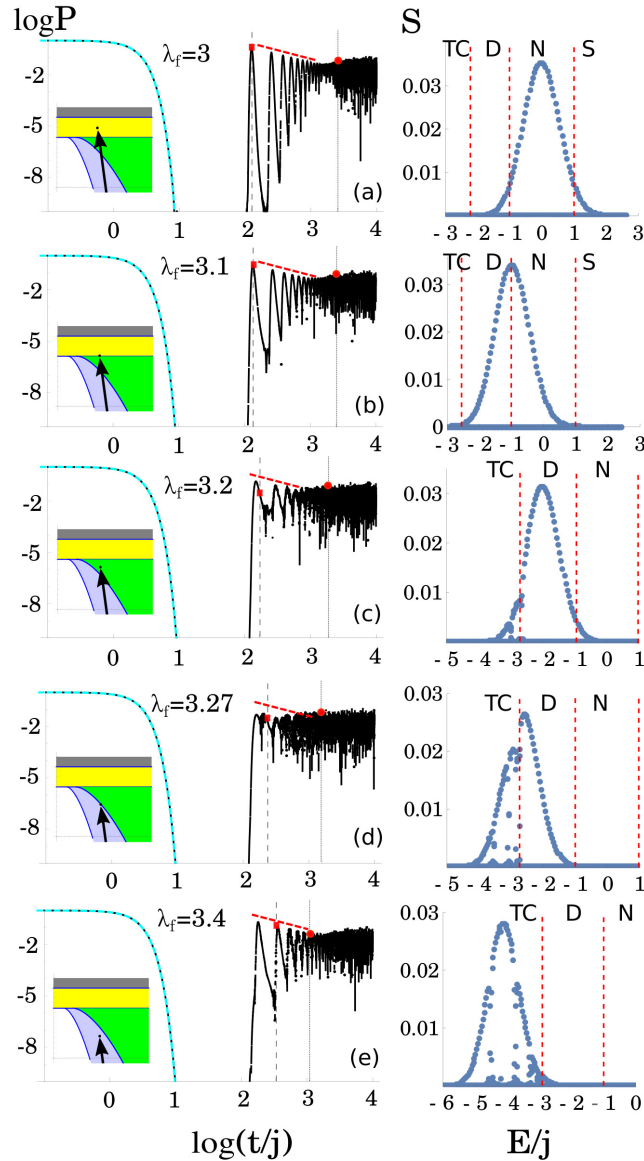


FIG. 8. (Color online) The Loschmidt echo and the strength function corresponding to the BQPs from the $\lambda_i = 6$ ground state of the $\delta = 0.3$ model with parameters $j = 20$, $\omega = \omega_0 = 1$ in the even parity sector. The standard and modified Heisenberg times t_H and t'_H are depicted with the red bullet and square, respectively. The $1/t$ decay of oscillations is marked with the red dashed lines.

In Fig. 10 the modified Heisenberg time t'_H and inverse participation ratio \mathcal{N}^{-1} are plotted for several values of λ_f . The dependence of t'_H has a maximum and \mathcal{N}^{-1} shows a dip close to the critical value $\lambda_f \doteq 3.27$ in a rough correspondence to the BQPs for $f = 1$ critical system, cf. Fig. 6. Note that the other critical value $\lambda_f = 3.1$ induces no effect on either t'_H or \mathcal{N}^{-1} .

If we increase the parameter δ , the overall degree of chaoticity involved in the model grows. Let us move on to probing the quench dynamics in the full Dicke model

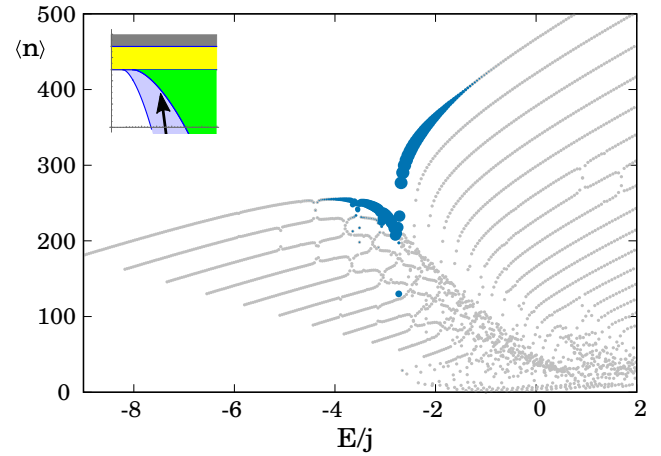


FIG. 9. (Color online) The Peres lattice with the average number of photons $\langle n \rangle$ for the $\lambda \doteq 3.27$, $\delta = 0.3$ Hamiltonian (the same parameters as in Fig. 8). The strength function from Fig. 8(d) is displayed by blue dots, the dot area encodes the respective $|s_l|^2$ value.

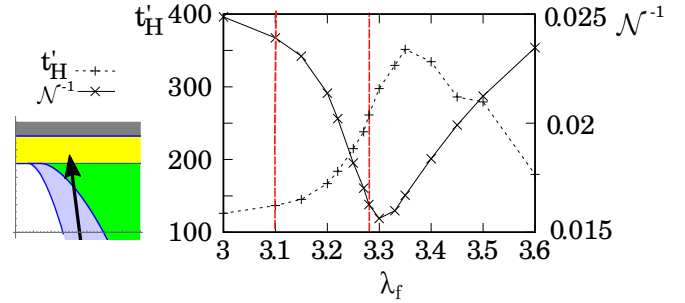


FIG. 10. (Color online) The modified Heisenberg time t'_H and inverse participation ratio \mathcal{N}^{-1} for the BQPs in the $\delta = 0.3$ model with the $\lambda_i = 6$ ground state. The parameters are the same as in Fig. 8. The critical quenches are marked with vertical lines. Lines connecting points serve as guides for eyes.

with $\delta = 1$. In Fig. 11, the Loschmidt echo is shown along with the respective strength function for several BQPs from the $\lambda_i = 4$ ground state. As λ_f we choose three values, with $\lambda_f = 2.06$ (panel b) corresponding to the critical quench to the $(f, r,) = (2, 1)$ ESQPT between the D and N phases.

As in Fig. 8, the initial decay for quenches in Fig. 11 is Gaussian. The revivals after the survival collapse can be partially fitted by the $1/t$ envelope in panel (c) whereas in panel (b) the oscillations are weakened and in panel (a) they are not present at all. This follows from the fact that the corresponding strength functions have much more complex structure compared to the $\delta = 0.3$ case. It is shown in Ref. [48] that if the strength function consists of several embedded Gaussian profiles (a clear example is panel c of Fig. 11), there are interference terms in the Loschmidt echo which distort the power-law decay.

The growing complexity of the strength function in-

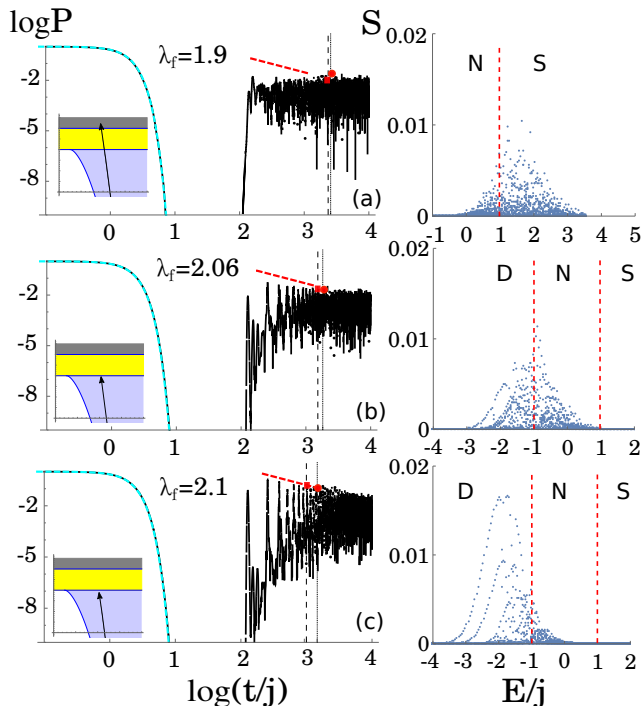


FIG. 11. (Color online) The Loschmidt echo and the strength function corresponding to the BQPs from $\lambda_i = 4$ ground state of the $\delta = 1$ model. The settings and symbols are the same as in Fig. 8.

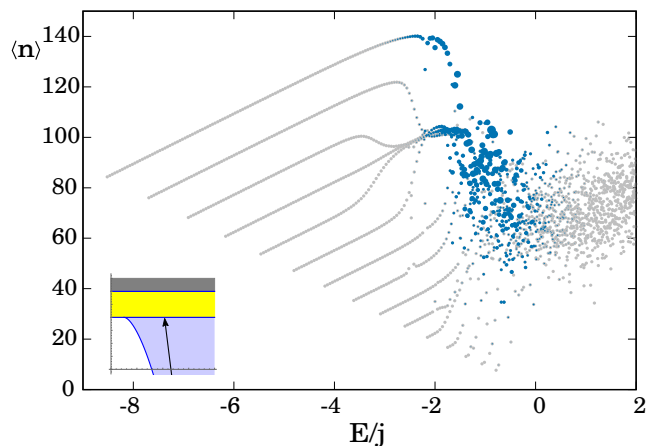


FIG. 12. (Color online) The Peres lattice as in Fig. 9 but for the $\lambda = 2.06$, $\delta = 1$ Hamiltonian. The strength function from Fig. 11(b) is depicted by blue dots.

indicates higher number of final eigenstates with non-zero $|s_l|^2$. In Fig. 12 we show the Peres lattice of the final spectrum for the critical quench $\lambda_f = 2.06$ with the strength function encoded in the size of blue points. We observe that the initial state is distributed mainly in the chaotic part of the spectrum. This is a radically different situation than for the critical quench to the same ESQPT

type with $\delta = 0.3$, cf. Fig. 9. Apparently, quantum chaos plays a dominant role in the disappearance of the power-law modulated revivals at $t \sim t_H$ smearing a possible ESQPT effects. Anyway, in Fig. 11(b) the presence of the ESQPT between D and N phases is still captured by the bimodality of the critical strength function.

Applying the same BQPs in the $\delta = 0.3$ and $\delta = 1$ versions of the model we attempt to identify some ESQPT-induced effects on the evolution of observables. We focus on the average number of photons $\langle n \rangle$, which is directly related to the photon flux leaving the cavity in the experimental setup described in Ref. [5]. Time evolution of $\langle n \rangle$ after the quench can be computed as

$$\langle n \rangle = \sum_l |s_l|^2 n_{ll} + 2 \sum_{l > l'} \text{Re}[s_l s_{l'}^* e^{i\omega_{ll'} t}] n_{ll'}, \quad (26)$$

where the star denotes complex conjugation, $\omega_{ll'} = E_{ll} - E_{l'l'}$, and $n_{ll'} = \langle \phi_{ll} | \hat{n} | \phi_{l'l'} \rangle$.

In Fig. 13 we present the results. In panels (a)–(c) the $\delta = 0.3$ case is depicted. The initial state is the superradiant ground state for $\lambda_i = 6$. The results are qualitatively similar as in the time evolution of the Loschmidt echo within the same BQPs, cf. Fig. 8. In non-critical cases (panels a and c in Fig. 13), the oscillations appear after the initial decay. These are further attenuated, so $\langle n \rangle$ reaches its saturation value given simply by the the first term in Eq. 26. In panel (b) where the critical quench is depicted, the oscillatory part of the evolution is suppressed, so the saturation regime is reached sooner. In other words, the time evolution of this observable captures the presence of ESQPTs in the same way as the Loschmidt echo does.

The time dependence of $\langle n \rangle$ after the quench in the $\delta = 1$ Dicke model is plotted in Fig. 13, panels (d)–(f). The critical quench is in panel (e). Similarly to the above described behavior of the Loschmidt echo, the ESQPT effect is suppressed due to a high degree of chaoticity.

IV. SUMMARY

We employed various types of quantum quench protocols in multiple settings of the extended Dicke model with the aim to test dynamical signatures of ESQPTs. Although the information in the time signal is often lost, effects of ESQPTs can be observed in the strength function which is an inverse Fourier transform of the Loschmidt echo. Nevertheless, in the protocols involving the ground states of the initial Hamiltonians, the effect is often visible even in the time dependences. We observed essentially two types of effects: either the stabilization of the initial state, or a speed-up of its decay.

In the context of the present model, the ESQPT-induced stabilization was observed in the class of forward quench protocols. It appears because the final Hamiltonian has a stationary point at the place of the initial Hamiltonian's global minimum. In our model, the stationary point is stable below the critical coupling (λ_c or

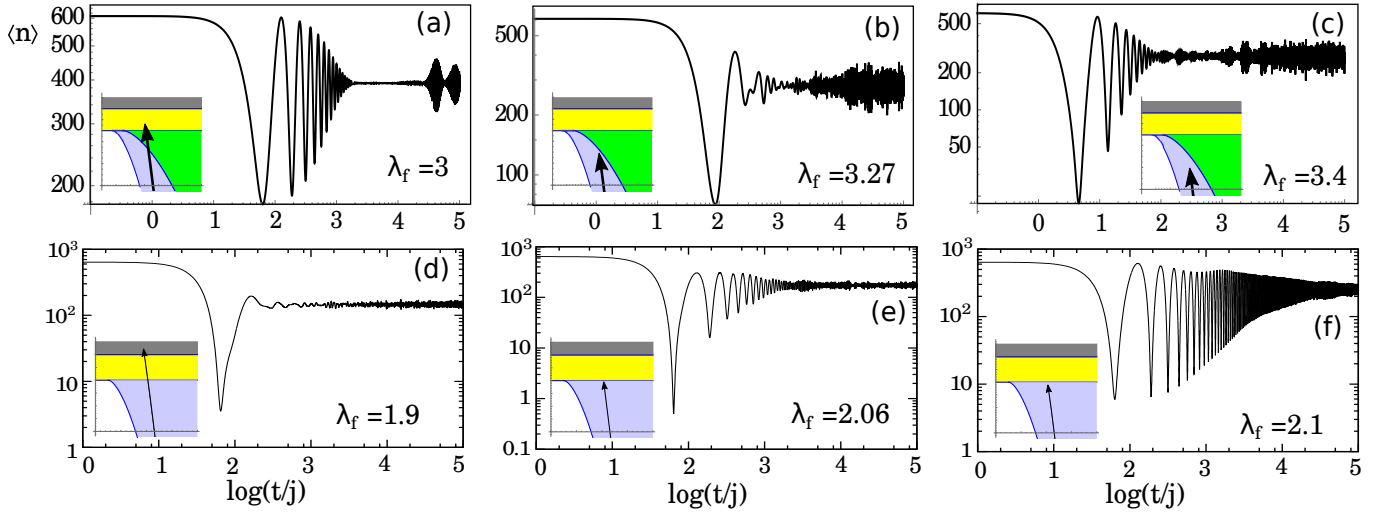


FIG. 13. (Color online) The time evolution of the average number of photons in the cavity $\langle n \rangle$ after the BQPs from the initial ground state. Panels (a)–(c) correspond to the $\delta = 0.3$ model with $\lambda_i = 6$ (the same quenches as in Fig 8). Panels (d)–(f) correspond to the $\delta = 1$ model with $\lambda_i = 4$ (the same quenches as in Fig 11). Other parameters are as in Fig. 8.

$\bar{\lambda}_c$) and unstable above (hence inducing an ESQPT). We examined three different cases:

- Integrable $\delta = 0$ model in its critical $M = 2j$ subspace. The unstable stationary point affecting the quenches with $\lambda_f \in (\bar{\lambda}_c, \infty)$ leads to the logarithmic divergence of the level density as in an ESQPT of the type $(f, r) = (1, 1)$. The stabilization effect was seen in Fig. 4(c).
- Non-integrable $\delta \in (0, 1]$ model. The unstable stationary point affecting quenches with $\lambda_f \in (\lambda_c, \lambda_0)$ constitutes an ESQPT with $(f, r) = (2, 1)$. The quench dynamics was shown in Fig. 7(a).
- Non-integrable $\delta \in (0, 1)$ model. The unstable stationary point affecting quenches with $\lambda_f \in [\lambda_0, \infty)$ constitutes an ESQPT with $(f, r) = (2, 2)$. In this case we observed even stronger stabilization due to nearly perfect localization of the strength function, see Fig. 7(b).

On the contrary, the ESQPT-induced speed-up of the decay of the initial state was observed in some backward quench protocols. The initial parameter value λ_i was chosen above the critical coupling (λ_c or $\bar{\lambda}_c$) and the parameter shift $\Delta\lambda$ was set such that the strength function was centered at the ESQPT energy. The speed-up is manifested as a disappearance or considerable suppression of the power-law stage of the quench dynamics at long time scales. The effect was clear in the following cases:

- Integrable $\delta = 0$ model in its critical $M = 2j$ subspace, see Fig. 5(b).

- Non-integrable $\delta \in (0, 1)$ model for quenches to the $(f, r) = (2, 1)$ ESQPT separating the D and TC phases, see Fig. 8(d).

The presence of the power-law decay at long time scales in the non-critical quenches is due to a combination of (a) Gaussian envelope of the strength function and (b) discrete sampling of the strength function with a quadratic variation of the level spacings. For the above specified critical quenches, this interplay is violated because of different quadratic dependences of level spacings on both sides of the ESQPT. Note that in both these cases the Heisenberg time (either t_H or t'_H) locally increases while the inverse participation ratio locally decreases, see Figs. 6 and 10.

The suppression of the power-law stage of the quench dynamic is not observed for quenches to ESQPTs of the type $(f, r) = (2, 2)$. Moreover, in the $\delta = 1$ model, the speed-up effect disappears even for $(f, r) = (2, 1)$ ESQPT. This is because the support of the strength function lies in the chaotic part of the final spectrum, cf. Figs. 9 and 12.

We have demonstrated that similar effects as in the Loschmidt echo can be detected in observables like the average photon number in the cavity. As seen in Fig. 13 this quantity shows a disappearance of the medium-time oscillations for critical quenches to the $(f, r) = (2, 1)$ ESQPT in $\delta \in (0, 1)$ model. This may suggest a way of experimental verification of ESQPT-related effects within a cold atom realization of the Dicke-like systems.

V. ACKNOWLEDGEMENT

We acknowledge funding of the Charles University in Prague under project UNCE/SCI/013.

-
- [1] C. Gardiner, P. Zoller, *The Quantum World of Ultra-Cold Atoms and Light*, Books I, II and III (Imperial College Press, London, 2014, 2015, 2016).
 - [2] I. M. Georgescu, S. Ashhab and F. Nori, *Rev. Mod. Phys.* **86**, 153 (2014).
 - [3] A. Gheorghiu, T. Kapourniotis and E. Kashefi, arXiv:1709.06984 [quant-ph] (2017).
 - [4] M. Greiner *et al.*, *Nature (London)* **415**, 39 (2002).
 - [5] K. Baumann *et al.*, *Nature* **464**, 1301 (2010); *Phys. Rev. Lett.* **107**, 140402 (2011).
 - [6] J. Klinder *et al.*, *Proc. Nat. Acad. Sci.* **112**, 3290 (2015).
 - [7] A. Polkovnikov *et al.*, *Rev. Mod. Phys.* **83**, 863 (2011).
 - [8] J. Eisert, M. Friesdorf and C. Gogolin, *Nature Phys.* **11**, 124 (2015).
 - [9] T. Gorin *et al.*, *Phys. Rep.* **435**, 33 (2006).
 - [10] A. Goussev *et al.*, *Scholarpedia*, 7(8):11687 (2012).
 - [11] A. Silva, *Phys. Rev. Lett* **101**, 120603 (2008).
 - [12] C. De Grandi, V. Gritsev and A. Polkovnikov, *Phys. Rev. A* **81**, 012303 (2010).
 - [13] P. Pérez-Fernández *et al.*, *Phys. Rev. A* **83**, 033802 (2011); *Phys. Rev. E*, 83 (2011).
 - [14] S. Montes and A. Hamma, *Phys. Rev. E* **86**, 021101 (2012).
 - [15] L. Campos Venuti and P. Zanardi, *Phys. Rev. A* **81**, 032113 (2010); *Phys. Rev. E* **89**, 022101 (2014).
 - [16] L.F. Santos and F. Pérez-Bernal, *Phys. Rev. A* **92**, 050101(R) (2015); L.F. Santos, M. Távora and F. Pérez-Bernal, *Phys. Rev. A* **94**, 012113 (2016).
 - [17] M. Heyl, *Rep. Prog. Phys.* **81**, 054001 (2018).
 - [18] R. Jafari and H. Johannesson, *Phys. Rev. Lett.* **118**, 015701 (2017).
 - [19] F. Pérez-Bernal and L.F. Santos, *Fortschr. Phys.* **65**, 1600035 (2017).
 - [20] M. Távora, E.J. Torres-Herrera and L.F. Santos, *Phys. Rev. A* **95**, 013604 (2017).
 - [21] E. J. Torres-Herrera, A. M. García-García, L. F. Santos, *Phys. Rev. B* **97** 060303(R) (2018).
 - [22] S. Sachdev, *Quantum Phase Transitions* (Cambridge Univ. Press, Cambridge, 2011).
 - [23] *Understanding Quantum Phase Transitions*, edited by L.D. Carr (CRC, Boca Raton, 2011).
 - [24] P. Cejnar *et al.*, *J. Phys. A: Math. Gen.* **39**, L515 (2006).
 - [25] M. Caprio, P. Cejnar, and F. Iachello, *Ann. Phys. (N.Y.)* **323**, 1106 (2008).
 - [26] P. Cejnar and P. Stránský, *Phys. Rev. E* **78**, 031130 (2008).
 - [27] P. Stránský, M. Macek, and P. Cejnar, *Ann. Phys. (N.Y.)* **345**, 73 (2014); P. Stránský *et al.*, *ibid.* **356**, 57 (2015).
 - [28] P. Stránský and P. Cejnar, *Phys. Lett. A* **380**, 2637 (2016).
 - [29] R.H. Dicke, *Phys. Rev.* **93**, 99 (1954).
 - [30] K. Hepp and E. H. Lieb, *Ann. Phys. (N.Y.)* **76**, 360 (1973).
 - [31] Y.K. Wang and F.T. Hioe, *Phys. Rev. A* **7**, 831 (1973).
 - [32] C. Emary and T. Brandes, *Phys. Rev. Lett.* **90**, 044101 (2003); *Phys. Rev. E* **67**, 066203 (2003).
 - [33] T. Brandes, *Phys. Rev. E* **88**, 032133 (2013).
 - [34] M.A. Bastarrachea-Magnani, S. Lerma-Hernández and J.G. Hirsch, *Phys. Rev. A* **89** 032101; 032102 (2014).
 - [35] M.A. Bastarrachea-Magnani, S. Lerma-Hernández and J.G. Hirsch, *J. Stat. Mech.* 093105 (2016).
 - [36] C.M. Lóbez and A. Relaño, *Phys. Rev. E* **94**, 012140 (2016).
 - [37] M. Kloc, P. Stránský, and P. Cejnar, *Ann. Phys. (N.Y.)* **382**, 85 (2017).
 - [38] M. Kloc, P. Stránský and P. Cejnar, *J. Phys. A: Math. Theor.* **50** 315205 (2017).
 - [39] M. Tavis and F. W. Cummings, *Phys. Rev* **170**, 379 (1968).
 - [40] F. Dimer *et al.*, *Phys. Rev. A* **75**, 013804 (2007).
 - [41] Z. Zhiqiang *et al.*, *Optica* **4**, 424 (2017).
 - [42] P. Cejnar and P. Stránský, *Phys. Scr.* **91**, 083006 (2016).
 - [43] F. Leyvraz and W.D. Heiss, *Phys. Rev. Lett.* **95**, 050402 (2005); P. Ribeiro, J. Vidal and R. Mosseri, *Phys. Rev. Lett.* **99**, 050402 (2007).
 - [44] A. Relaño *et al.*, *Phys. Rev. A* **78**, 060102(R) (2008).
 - [45] V.M. Bastidas *et al.*, *Phys. Rev. Lett.* **112**, 140408 (2014).
 - [46] W. Kopylov and T. Brandes, *New J. Phys.* **17**, 103031 (2015).
 - [47] P. Bocchieri and A. Loinger, *Phys. Rev.* **107**, 337 (1957); L.S. Schulman, *Phys. Rev. A* **18**, 2379 (1978).
 - [48] S. Lerma-Hernández *et al.*, arXiv:1710.05937 [quant-ph] (2017).
 - [49] A. Peres, *Phys. Rev. Lett.* **77**, 1413 (1996).
 - [50] P. Stránský, P. Hruška, P. Cejnar, *Phys. Rev. E* **79**, 066201 (2009).